# Image Up-Sampling Using Total-Variation Regularization With a New Observation Model

Hussein A. Aly, *Member, IEEE,* and Eric Dubois, *Fellow, IEEE*

***Abstract*—This paper presents a new formulation of the regularized image up-sampling problem that incorporates models of the image acquisition and display processes. We give a new analytic perspective that justifies the use of total-variation regularization from a signal processing perspective, based on an analysis that specifies the requirements of edge-directed filtering. This approach leads to a new data fidelity term that has been coupled with a total-variation regularizer to yield our objective function. This objective function is minimized using a level-sets motion that is based on the level-set method, with two types of motion that interact simultaneously. A new choice of these motions leads to a stable solution scheme that has a unique minimum. One aspect of the human visual system, perceptual uniformity, is treated in accordance with the linear nature of the data fidelity term. The method was implemented and has been verified to provide improved results, yielding crisp edges without introducing ringing or other artifacts.**

***Index Terms*—Data fidelity, gamma correction, image up-sampling, interpolation, level-sets motion (LSM), observation model, regularization, total variation.**

## I. Introduction

DIGITAL-image magnification with higher perceived resolution is of great interest for many applications, such as law enforcement and surveillance, standards conversions for broadcasting, printing, aerial- and satellite-image zooming, and texture mapping in computer graphics. In such applications, a continuous real-world scene is projected by an ideal (pin-hole) optical system onto an image plane and cropped to a rectangle $\mathcal{W}$. The resulting continuous image $f_c$ is acquired by a physical camera to produce a digital lower resolution (LR) image $f_2$ (i.e., lower than desired) defined on a lattice $\Gamma$ (following the notation of [1], [2]). This camera, including the actual optical component, is modeled as shown in Fig. 1 as a continuous-space filter $h_2$ followed by ideal sampling on $\Gamma$. The problem dealt with in this paper is, given the still LR image $f_2$, obtain the best perceived higher resolution (HR) image defined on a denser sampling lattice $\Lambda$. Here, we hypothesize that an ideal HR image $f_1$ defined on a denser lattice $\Lambda$ can be obtained in principle directly from $f_c$ by a virtual camera, which can similarly be modeled by filtering with a continuous-space filter $h_1$ followed by ideal sampling on $\Lambda$. Our goal is then to obtain an estimate of $f_1$ denoted by $\hat{f}_1$ with the highest perceptual quality.

Many solution methods for the image magnification problem exist in the literature, with a broad quality range. We can categorize these solution methods into model-based and non-model-based ones. Non-model-based methods use linear or nonlinear (adaptive) interpolation. Linear interpolators range from straightforward pixel repeat [which is also called zero-order hold (ZOH)], bilinear, or bicubic [3] interpolation to embedding in spline kernel spaces [4]–[7]. Simple linear methods suffer from staircasing (blocking) of oblique edges, blurring of the object boundaries and texture, and ringing in smooth regions that are adjacent to edges. Splines produce better quality up-sampled images than those obtained by straightforward linear interpolators, but are known to produce oscillatory edges with significant ringing near them. Analysis of this effect based on image isophotes (iso-intensity contours) can be found in [8]. These drawbacks of the linear methods have led to research in adaptive methods, whose goal is to preserve the sharpness of strong edges in the up-sampled image $\hat{f}_1$. They adapt the interpolation method used according to the edges given in the LR image and, hence, are generally called edge-directed interpolation [9]–[12]. Another nonlinear approach exploits local correlation of the samples without explicitly extracting edges by defining a local metric that determines the local participation weight of each sample of $f_2$ in interpolating a sample of $\hat{f}_1$ [13]–[17]. Adaptive methods can produce clearly visible edges as compared to those produced by the linear class, enhancing the overall perceived quality of the resulting images. However, this class has the drawbacks of relying on good edge estimation or local correlation and every implementation is sensitive to the orientations of the edges. Despite the fact that the sharpness of the edges is being enhanced by adaptive methods, the crispness of long edges is not well handled and they are usually wavy, and blotching occurs on the boundaries of edges. Furthermore, there is no solid theoretical base that unifies the realization of the approaches of this class and every approach stands on its own.

Model-based image up-sampling methods rely on modeling the imaging processes and using sophisticated regularization methods describing *a priori* constraints. According to the formulation of Fig. 1, it can be shown that $f_2$ can be related to $f_1$ by down-sampling, as shown in Fig. 2 [18], or, more generally, by arbitrary rate conversion in the case of $\Gamma \nsubseteq \Lambda$. Without loss of generality, we only consider the case of $\Gamma \subseteq \Lambda$; the more general case can be handled by an up-sampling step to an inter-

Manuscript received March 13, 2004; revised September 14, 2004. This work was supported in part by the Ministry of Defence, Egypt, and in part by the Natural Sciences and Engineering Research Council of Canada. The associate editor coordinating the review of this manuscript and approving it for publication was Dr. Thierry Blu.

H. A. Aly is with the Ministry of Defence, Cairo, Egypt (e-mail: haly@ieee.org).

E. Dubois is with the School of Information Technology and Engineering, University of Ottawa, Ottawa, ON K1N 6N5 Canada (e-mail: edubois@uottawa.ca).

Digital Object Identifier 10.1109/TIP.2005.851684

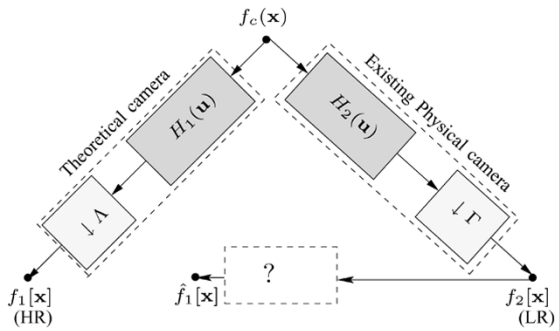


Fig. 1. Formulation of the image up-sampling problem based on models of the physical lower resolution camera and the theoretical higher resolution camera.

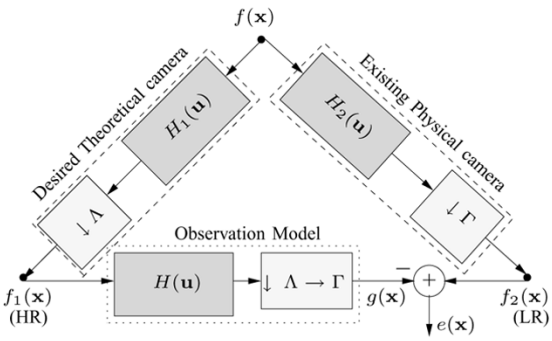


Fig. 2. Definition of the observation model in context of the formulation of Fig. 1.

mediate super-lattice. If we stack rows of $f_1$ and $f_2$ into lexicographic column vectors, then we can describe the relation by

$$\mathbf{f}_2 = H\mathbf{f}_1 \tag{1}$$

where $H$ is a sparse matrix that combines both filtering and down-sampling processes. The number of rows of $H$ is equal to the number of samples in $f_2$ and the number of columns is equal to the number of samples in $f_1$. It is clear that $H$ has a nonzero null space with $\dim(\mathrm{Null}(H)) > 0$ [19]. This means that all the components of $f_1$ that lie in $\mathrm{Null}(H)$ will not be observed in $f_2$. These components are the high frequencies in $f_1$ that are perceived as fine details. Since our problem here is to obtain $\hat{f}_1$ from $f_2$, we want to "undo" the transformation given by (1), which is mathematically called an inverse problem. Hadamard [20] defined a problem to be well posed if there *exists* a solution for it that is *unique* and depends *continuously* on the data. In our case here, the *uniqueness is violated*; indeed, many different images $f_1$ can produce the same $f_2$ using (1) because when their differences lie in $\mathrm{Null}(H)$ they will not appear at all in $f_2$. This classifies our problem as an *ill-posed* inverse problem. Specifically, (1) describes an under-determined linear system that has an infinite number of possible inverse solutions for $\hat{\mathbf{f}}_1$. This ill-posed inverse problem when approached in a regularization-based framework would generally be formulated as an optimization problem. Two cost functions are set: a data fidelity to the observed LR image $\mathcal{J}_d(\hat{f}_1, f_2)$ that penalizes inconsistency between the estimated HR image and the observed LR image, and a regularizer (*a priori* constraints) $\mathcal{J}_s(\hat{f}_1)$. Thus, in model-based methods, the problem of obtaining an HR image estimate $\hat{f}_1$ is given by

$$\hat{f}_1 = \arg\min_f \{\mathcal{J}_d(f, f_2) + \lambda \mathcal{J}_s(f)\} \tag{2}$$

where $\lambda$ is a regularization parameter that controls the tradeoff between $\mathcal{J}_d$ and $\mathcal{J}_s$.

The role of regularization is to incorporate additional *a priori* knowledge about the problem, convert an ill-posed problem to become a well-posed one, or select one of the infinite number of possible solutions described by (1). Regularization has been used in many image-processing problems such as restoration, enhancement, motion estimation, magnification with better perceived resolution, etc. Examples of some popular regularizers are generalized inverse (minimum energy), c-generalized inverse (*Tikhonov*), statistical approaches [*maximum a posteriori* (MAP) estimation] especially using a Markov random field *a priori* image model [21]–[24] and total variation [25], [26]. A survey of the most widely used regularizers in image processing can be found in [27].

In this paper, we present a new formulation and analysis for the image up-sampling problem justifying the use of the total-variation regularizer. At the formulation level we use two ingredients: a new observation model and the total-variation regularizer. The formulation is set as an optimization problem and is numerically solved by a level-sets motion (LSM) algorithm. The numerical implementation of the LSM involves a new selection of two hybrid motions for the evolution that has resulted in a better solution method than the previously reported implementations. The results show superior magnified images compared to other state-of-the-art methods.

The rest of the paper is organized as follows. In Section II, we provide our analytic perspective about the problem of image up-sampling and establish the link to the total-variation regularizer from a signal processing perspective. We conclude the section with background material on the level-set method and LSM. Section III provides the details and design of the data fidelity metric. We present our proposed image up-sampling scheme in Section IV with the associated design of the hybrid speeds for the LSM that represents a novel design providing a stable solution scheme. A conflicting aspect of perceptual uniformity and the linear nature of the data fidelity term is presented and resolved with a new methodology in Section V. Detailed implementation algorithms are presented in Section VI including methods for estimation of the partial derivatives. A new estimation method is also given in this section. We present our experiments and results in Section VII for up-sampling of several images, with comparisons to other methods from the literature. Finally, we conclude the paper in Section VIII.

## II. Analytic Perspective and Motivations

In order to adequately formulate the problem with a suitable regularization method, we need to perform an in-depth analysis, define our requirements, and find the best regularizer that can achieve these requirements in a suitable manner. We perform our analysis in the frequency domain. Assume that $f_c$ has a continuous-space Fourier transform $F_c(\mathbf{u}) = \int_{\mathbb{R}^D} f_c(\mathbf{x}) \exp(-j2\pi \mathbf{u} \cdot \mathbf{x})\, d\mathbf{x}$, where $D = 2$ for still images and $D = 3$ for time-varying

images, and "$\cdot$" denotes inner product. A signal $f$ with finite energy defined on a lattice $\Lambda$ is denoted by $f \in \ell^2(\Lambda)$ and has a Fourier transform $F(\mathbf{u}) = \sum_{\mathbf{x}\in\Lambda} f[\mathbf{x}] \exp(-j2\pi \mathbf{u}\cdot\mathbf{x})$. The Fourier transform $F(\mathbf{u})$ is periodic in the frequency domain, i.e., $F(\mathbf{u}+\mathbf{r}) = F(\mathbf{u}), \forall \mathbf{r} \in \Lambda^*$, where $\Lambda^*$ is the reciprocal lattice to $\Lambda$ [2]; any unit cell of $\Lambda^*$, denoted $\mathcal{P}_{\Lambda^*}$, constitutes one period of $F(\mathbf{u})$. It should be noted that if $\Lambda$ is generated by a sampling matrix $V_\Lambda = [\mathbf{v}_1 \,|\, \mathbf{v}_2 \,|\, \cdots \,|\, \mathbf{v}_D]$, where the column vectors $\mathbf{v}_i, i = 1, \ldots, D$ are the linearly independent basis vectors of the lattice $\Lambda = \mathrm{LAT}(V_\Lambda) \triangleq \{V_\Lambda \mathbf{n} : \mathbf{n} \in \mathbb{Z}^D\}$, then the reciprocal lattice is $\Lambda^* = \mathrm{LAT}(V_\Lambda^{-\mathrm{T}})$, where the superscript $-\mathrm{T}$ denotes the transpose of the matrix inverse.

### A. Problem of Nonbandlimited Images

As shown in Fig. 1, $f_2$ is acquired by a physical camera which in practice is not well-modeled by an ideal low-pass prefiltering ($h_2$) of the continuous image $f_c$. Consequently, the continuous-space filtering by $h_2$ does not confine the spectrum $F_c(\mathbf{u})$ to a unit-cell $\mathcal{P}_{\Gamma^*}$, and aliasing will be introduced by the sampling process on $\Gamma$. This is true for natural images $f_c$ because they are not bandlimited and current physical cameras because they do not model an ideal low-pass prefilter. This leads to the first fact that the spectrum $F_2(\mathbf{u})$ is nonnegligible at the border of $\mathcal{P}_{\Gamma^*}$. This is illustrated in Fig. 3, which shows an estimate of the power spectral density (PSD) of a version of the familiar Massachusetts Institute of Technology (MIT) cameraman image (a portion of which is shown in Fig. 8) which was obtained by scanning an original photographic print of size $6 \times 6$ in at 75 dots-per-inch (dpi) producing a $450 \times 450$-pixel image. This PSD was estimated using the Welch-modified-periodogram method [28] with a Blackman–Harris window [29]. Concerning the problem of image up-sampling to obtain $\hat{f}_1$, if we hypothesize that we have an ideal sinc interpolation, then a sharp cutoff by the ideal low-pass filter interpolator will introduce a very sharp frequency transition in the spectrum of $F_1(\mathbf{u})$ *inside* the band $\mathcal{P}_{\Lambda^*}$ (and not at its border). Specifically, this sharp frequency transition will be at the location of the border of $\mathcal{P}_{\Gamma^*}$ in $\mathcal{P}_{\Lambda^*}$. This in-band sharp frequency transition has the effect of introducing spatially infinite trailing oscillations as is known for the sinc function. On the other hand, linear filters such as ZOH, bilinear, bicubic interpolators will generally leave nonnegligible undesired replicas of the spectrum $F_2(\mathbf{u})$ in $\mathcal{P}_{\Lambda^*} \setminus \mathcal{P}_{\Gamma^*}$, resulting in the artifacts described in Seciton I. Since we know that there are aliasing components in $F_2(\mathbf{u})$, then we desire to use them to re-synthesize or extrapolate $F_1(\mathbf{u})$ in $\mathcal{P}_{\Lambda^*} \setminus \mathcal{P}_{\Gamma^*}$ in a consistent manner to $F_2(\mathbf{u})$ to provide the best perceived image $\hat{f}_1$.

### B. Specifying the Requirements

Maintaining the sharpness of edges in an up-sampled image $\hat{f}_1$ corresponds to synthesizing new useful high-frequency components in $\hat{F}_1(\mathbf{u})$ consistent with, but beyond, those existing in its counterpart $F_2(\mathbf{u})$. Conceptually, this is locally achievable by interpolating *along* the edges or isophotes, while avoiding interpolation *across* them. Furthermore, we want to achieve this concept by formulating a global criterion rather than using an edge-detector coupled with an ad-hoc local pixel classifier. The

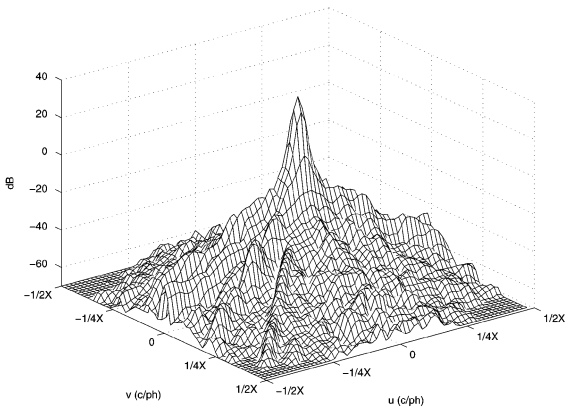


Fig. 3. Estimate of the PSD of the cameraman image.

situation is depicted in the frequency domain in Fig. 4, where a sample edge with a specific spatial orientation is superimposed on the profile of its frequency spectrum. It is straightforward to deduce that the orientation of the profile of the spectrum of an edge will maintain a local orthogonality to the edge orientation. The figure shows how linear interpolators, such as ZOH, bilinear, or higher order filters, introduce artifacts due to inclusion of undesired spectral replicas from adjacent unit cells, which is the worst for diagonal edges. The figure shows how a locally edge-directed (directionally oriented) filter can effectively extract all the spectrum of the edge (no blurring) without including any portion of the adjacent spectral replicas (which cause staircasing and ringing). The idea can be extended for all isophotes at all locations,[1] giving rise to a space-variant filter that is dependent on the underlying data.

### C. Total-Variation Regularizer

*Variational* approaches have been applied for image restoration and denoising in several forms such as anisotropic diffusion [30], total variation [31], and mean-curvature evolution [32]. All of these formulations are different forms of a unified functional form of the variational regularizer given by

$$\mathcal{J}_s(f) = \int_{\mathcal{W}} \mathfrak{L}(\|\nabla_{\mathbf{x}} f(\mathbf{x})\|)\, d\mathbf{x}. \tag{3}$$

If we assume that we have a continuous version $f$ constructed from the samples of the estimate $\hat{f}_1$, then the regularizer for this continuous image is defined on $\mathcal{W}$, and $\nabla_{\mathbf{x}}$ denotes the spatial gradient. The functional $\mathfrak{L}$ is nonnegative, monotonically increasing, and its derivative $\mathfrak{L}'(\cdot) > 0$ except for $\mathfrak{L}'(0) = 0$ [33]. A trivial minimizer for (3) is the set of all constant images $f$. However, a data fidelity $\mathcal{J}_d$ to a given LR image is always coupled to $\mathcal{J}_s$, as shown in (2). In this sense, the minimization of (3) is more arduous and is solved as a problem of calculus of variations [34]. Using Euler's equation, the minimizer is the steady-state solution of the nonlinear parabolic [35] partial differential equation (PDE) given by

$$\frac{\partial f}{\partial \tilde{t}} = \mathrm{div}\left( \frac{\mathfrak{L}'(\|\nabla_{\mathbf{x}} f(\mathbf{x}, \tilde{t})\|)}{\|\nabla_{\mathbf{x}} f(\mathbf{x}, \tilde{t})\|} \nabla_{\mathbf{x}} f(\mathbf{x}, \tilde{t}) \right). \tag{4}$$

[1]Edge-directed interpolation methods try to apply the concept for strong edges only because they rely on an edge-detection stage before applying a simple linear interpolation method along these detected edges.

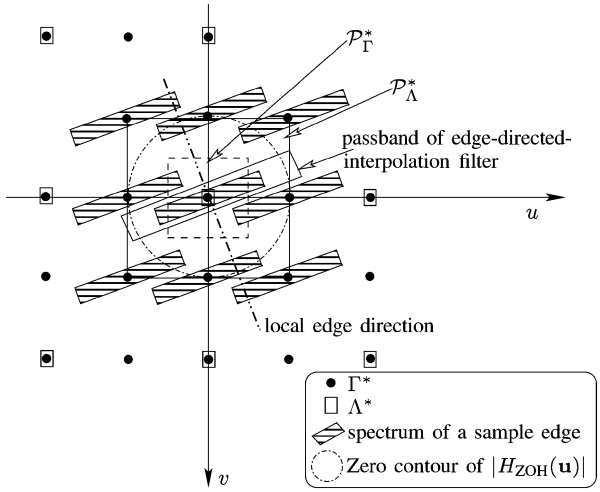


Fig. 4. Illustration of edge-directed interpolation for a sample edge.

Here, $\tilde{t}$ is an *artificial time* parameter for the evolution process of this initial value problem and div denotes the divergence operator. Factoring the divergence operator, or using the eigenvalue decomposition of the Hessian of $\mathfrak{L}(\|\nabla_{\mathbf{x}} f\|)$ as done in [33], we obtain

$$\frac{\partial f}{\partial \tilde{t}} = \frac{\mathfrak{L}'(\|\nabla_{\mathbf{x}} f(\mathbf{x},\tilde{t})\|)}{\|\nabla_{\mathbf{x}} f(\mathbf{x},\tilde{t})\|}\|\nabla_{\mathbf{x}} f(\mathbf{x},\tilde{t})\|\kappa + \mathfrak{L}''(\|\nabla_{\mathbf{x}} f(\mathbf{x},\tilde{t})\|)\|\nabla_{\mathbf{x}} f(\mathbf{x},\tilde{t})\|\kappa^{\perp}. \quad (5)$$

At a specific artificial time instant, $\kappa$ is the mean curvature of $f$, and $\kappa^{\perp}$ can be thought as the dual mean curvature [33]. In other words, $\|\nabla_{\mathbf{x}} f(\mathbf{x},\tilde{t})\|\kappa$ is the second-order directional derivative in the direction that is orthogonal to the gradient $\nabla_{\mathbf{x}} f$, and $\|\nabla_{\mathbf{x}} f(\mathbf{x},\tilde{t})\|\kappa^{\perp}$ is the second-order directional derivative in the direction of the gradient $\nabla_{\mathbf{x}} f$. The geometric interpretation of (5) is very interesting and sheds light on the dynamics of variational regularizers. The evolution process in the artificial time $\tilde{t}$ given by (5) is seen as an energy dissipation process in two orthogonal directions. This dissipation process diffuses $f(\mathbf{x},\tilde{t})$ along the direction of the gradient and along the orthogonal direction to the gradient. The diffusion process of the grey-values of $f(\mathbf{x},\tilde{t})$ along the direction of the spatial gradient (orthogonal to the image contours) is seen as a kind of averaging across both sides of the local image contour. This has the effect of blurring contours and smoothing the image as in the case of linear interpolators, which is an *undesirable* action in our case here according to Fig. 4 and should be suppressed. The diffusion process of $f(\mathbf{x},\tilde{t})$ along the orthogonal direction to the gradient (along the image contours) is seen as isophote-directed filtering. This will preserve the location and the intensity transitions of the contours, while smoothing along them maintaining their crispness, which represents our *desirable* requirement. Both requirements can be fulfilled if we let $\mathfrak{L}''(\cdot)$ vanish while maintaining a nonzero $\mathfrak{L}'(\cdot)$. Intuitively, it seems that choosing $\mathfrak{L}(\cdot)$ as a nonzero linear function will do the job. This means that a possible desirable function is $\mathfrak{L}(\|\nabla_{\mathbf{x}} f\|) = \|\nabla_{\mathbf{x}} f\|$. This choice leads to the evolution process given by

$$\frac{\partial f}{\partial \tilde{t}} = \kappa = \mathrm{div}\left(\frac{\nabla_{\mathbf{x}} f(\mathbf{x},\tilde{t})}{\|\nabla_{\mathbf{x}} f(\mathbf{x},\tilde{t})\|}\right). \quad (6)$$

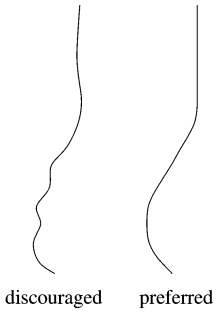


Fig. 5. Total-variation regularization discourages oscillatory isophotes.

This is exactly the evolution process introduced by Rudin *et al.* in [31] for image denoising and restoration. The above analysis provides sufficient evidence regarding the success one would expect using the total-variational regularizer; more details and the relation to Tikhonov regularization can be found in [36].

The minimization of the total-variation regularizer $\mathcal{J}_s(f) = \int_{\mathcal{W}} \|\nabla_{\mathbf{x}} f(\mathbf{x})\|\, d\mathbf{x}$ that we have chosen in this paper has also unique mathematical interpretations.

- It favors signals that have bounded variations without penalizing possible discontinuities. This is a suitable space for natural images because they usually contain sharp discontinuities at the borders separating different objects. It should be noted that it does not favor sharp edges to blurry ones because both have the same total variation, but it will preserve sharpness of edges in the given observation [37];
- Its minimizer is an image which has the least oscillatory iso-intensity contours as shown in Fig. 5. This means that the solution with smooth contours is preferable to oscillatory or jagged solutions. This is desirable in maintaining edges with smooth isophotes when this agrees with the observed data in the LR image.

From a signal processing perspective, the evolution process given by (6) is fully an implicit local isophote-directed processing that is performed without the need for any explicit edge detection technique. This evolution process has been well analyzed mathematically and geometrically, and we have the available stability analysis and numerical techniques for it through the concept of level sets and propagation of fronts.

In the case of spatiotemporal data ($D = 3$), the idea of edge-directed interpolation, coupled with motion estimation, can be applied along the motion trajectories. Hence, a three-dimensional total variation can be used to smooth the objects along their trajectories, while not penalizing temporal discontinuities such as occlusions, or objects newly introduced and disappearing from the scene.

### D. Background on LSM and Propagation of Fronts

Propagation (evolution) of fronts at a certain spatially variant speed along the normal direction to the front has been studied by Osher and Sethian [38]. Specifically, they analyzed the problem for fronts propagating with a speed that is dependent on the curvature of the front. They developed a numerical scheme for

tracking the front as it propagates, naming it later as the level set method, and gave its general form by

$$\frac{\partial \Psi(\mathbf{x},\tilde{t})}{\partial \tilde{t}} + \nu(\mathbf{x},\tilde{t})\|\nabla_{\mathbf{x}}\Psi(\mathbf{x},\tilde{t})\| = 0 \tag{7}$$

where $\nu(\cdot)$ is the speed of the evolution along the normal direction to the front. The front is defined in terms of a higher dimensional embedding function $\Psi$ as the set $\Psi(\mathbf{x},\tilde{t}) = 0$. Several types of evolutions (motions) are described by the properties of the speed $\nu$ in [39].

Images can be represented by their iso-intensity contours, i.e., contours that have equal grayscale value (*isophotes*); hence, an image $f$ is a collection of its level-sets. If we let the image level-sets (isophotes) propagate with different types of motion with special characteristics, then we can obtain results such as straightening out oscillatory contours, shrinking an isolated noise component within a smooth region so that it vanishes (as in morphological operations), preserving the boundaries of small objects, etc.; more details can be found in [36].

The LSM of an image $f$ is not to be confused with the level set method for tracking a specific front; in other words, LSM of $f$ does not imply that $f$ is a higher dimensional function $\Psi$ as given by (7). Here, the numerical implementation of the LSM of an image $f$ is based on the well-established numerical scheme of the level set method. In that sense, an LSM for image deblurring and noise removal is given in [40].

## III. Data Fidelity

Much research has focused on designing the regularizer $\mathcal{J}_s$, whereas $\mathcal{J}_d$ has not received a similar level of in-depth analysis. According to (1), the straightforward objective criterion normally used is formulated in the classical least-squares sense as

$$\hat{\mathbf{f}}_1 = \arg\min_{\mathbf{f}} \mathcal{J}_d(\mathbf{f},\mathbf{f}_2),$$
$$\mathcal{J}_d(\mathbf{f},\mathbf{f}_2) = \frac{1}{2}\|H\mathbf{f} - \mathbf{f}_2\|^2. \tag{8}$$

This criterion is known as the *data fidelity* term[2] which depends on the matrix H or specifically the digital filter $h$ as shown in Fig. 2. Simple models for $h$ such as the moving average introduced in [21] have been used for most image interpolation and super-resolution research [23], [41]. Baker and Kanade [42] involved in their analysis a general form for the optical blurring effect convolved with a rectangular function that models a CCD camera used to acquire the LR image. In all the variational formulations for image up-sampling, the two sampling structures $\Lambda$ and $\Gamma$, having different densities, were not simultaneously considered. Instead, the design of $\mathcal{J}_d$ only involved images that are defined on the same lattice, either $\Gamma$ or $\Lambda$. In [43]–[47], $\mathcal{J}_d$ was only designed on $\Gamma$ by assuming that the filter $h$ shown in Fig. 2 is a unit-sample impulse leaving most of the samples of $f_1$ unconstrained. In [25], $\mathcal{J}_d$ was defined on $\Lambda$ only by up-sampling the LR image $f_2$ using an interpolator whose frequency profile is as that of the ideal low-pass filter (sinc). The problem became one of restoration and ringing was dealt with using the total-variation regularizer.

We designed an accurate $h$ in [18] based on the properties of the physical and theoretical camera prefilters $h_2$ and $h_1$, respectively, as shown in Fig. 2. The motivation for the study in [18] is that an accurate observation model leads to a better definition of the solution space which is indeed a critical factor for a better quality up-sampling [48]. It was found that the optimal filter has the closed form $\mathbf{h} = -0.5D^{-1}\mathbf{b}$, where the elements of $\mathbf{b}$ and the matrix $D$ are both functions of $h_1, h_2$, and the PSD of $f_c$ [18]. In this paper, we assume that the theoretical and physical cameras are described by certain scenarios that define $h_1, h_2$, and the ratio of the densities of both lattices $\Lambda$ and $\Gamma$, and we obtain the optimum filter $h$ using the method described in [18].

## IV. Proposed Method for Grayscale Image Up-Sampling

Our preliminary work in [49] provides a variational formulation for the image up-sampling problem that involves two different sampling structures $(\Lambda,\Gamma)$ simultaneously in the formulation and the solution. Our proposed formulation for regularized grayscale image up-sampling is given by

$$\begin{aligned}&\hat{\mathbf{f}}_1 = \arg\min_{\mathbf{g}}\left\{\tfrac{1}{2}\|H\mathbf{g} - \mathbf{f}_2\|^2 + \lambda \textstyle\int_{\mathcal{W}} \|\nabla_{\mathbf{x}}(g_\varphi)(\mathbf{x})\|\, d\mathbf{x}\right\}\\ &(g_\varphi)(\mathbf{x}) \triangleq \textstyle\sum_{\mathbf{d}\in\Lambda} g[\mathbf{d}]\varphi(\mathbf{x}-\mathbf{d}), \quad \forall \mathbf{x}\in\mathcal{W}\\ &g\in\ell^2(\Lambda), \quad f_2\in\ell^2(\Gamma), \quad (g_\varphi)\in L^2(\mathcal{W}).\end{aligned} \tag{9}$$

The prototype continuous function $\varphi$ embeds a discrete image defined on $\Lambda$ into $L^2(\mathcal{W})$. An LSM is presented to solve the above proposed formulation. We used two types of motions with different spatially variant speeds that interact simultaneously to provide the solution for (9). These two motions are proposed to have the speeds

$$\begin{aligned}\nu_s &= -\lambda\kappa(\mathbf{x},\tilde{t}),\\ \nu_d &= \left(\frac{r_\varphi}{\|\nabla_{\mathbf{x}}(f)\|}\right)(\mathbf{x},\tilde{t})\end{aligned} \tag{10}$$

where the residue $r \in \ell^2(\Lambda)$ is the inverse lexicographical reordering of the lexicographic vector $H^{\mathrm{T}}(H\mathbf{f} - \mathbf{f}_2)$. The matrix $H^{\mathrm{T}}$ performs both the up-sampling operation from $\Gamma$ to $\Lambda$ followed by filtering with the time-reversal filter $h[-\mathbf{x}]$. Let us define $f_\kappa[\mathbf{x}] \triangleq (\|\nabla_{\mathbf{x}}(f_\varphi)\|\kappa)(\mathbf{x}), \forall \mathbf{x} \in \Lambda$. We solve (9) by an LSM as the steady state solution of $\partial f(\mathbf{x},\tilde{t})/(\partial\tilde{t}) + \nu(\mathbf{x},\tilde{t})\|\nabla_{\mathbf{x}} f(\mathbf{x},\tilde{t})\| = 0$ for $\nu = \nu_s + \nu_d$. The numerical implementation of the artificial time derivative is given as in the level-set method by the forward Euler method as $\partial f/\partial\tilde{t} = (f^{(n+1)} - f^{(n)})/\Delta T$, where $\Delta T$ is a time step and the superscript $(n)$ denotes the iteration index. Using the numerical schemes of the level set method, we obtain our iterative up-sampling method as

$$\hat{\mathbf{f}}_1^{(n+1)} = \left[\hat{\mathbf{f}}_1 + \Delta T\left(\lambda\hat{\mathbf{f}}_{1_\kappa} - H^{\mathrm{T}}(H\hat{\mathbf{f}}_1 - \mathbf{f}_2)\right)\right]^{(n)} \tag{11}$$

where $\kappa = (f_{xx}f_y^2 - 2f_xf_yf_{xy} + f_{yy}f_x^2)/(f_x^2+f_y^2)^{3/2}$, $f_{(\cdot)}$ denotes the partial derivative with respect to "$(\cdot)$," and the square brackets with the superscript $(n)$ denotes that all the included

[2]This $1/2$ is just for convenience for later evaluation of the derivatives and has no impact on the objective criterion.

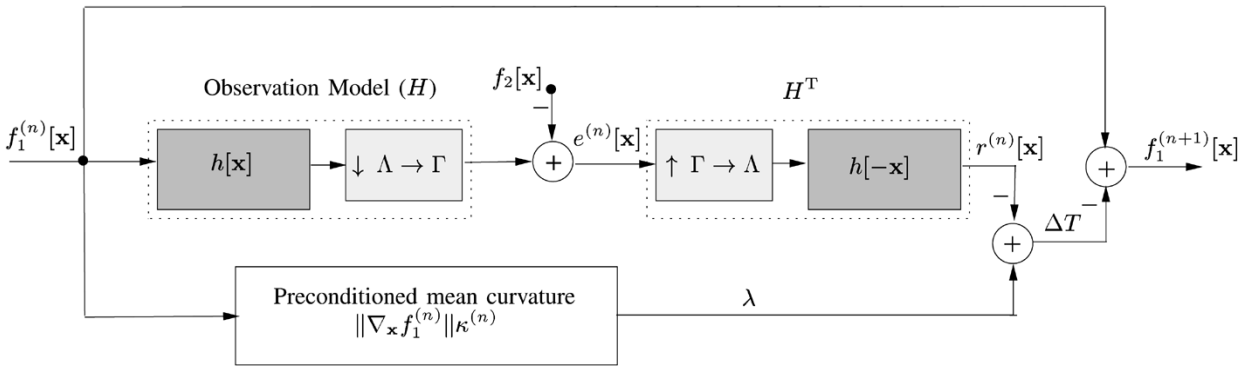


Fig. 6. Block diagram showing implementation of one iteration of the up-sampling algorithm (1).

occurrences of $f_1$ are its value at iteration $n$. Equation (11) represents an evolution under the preconditioned mean curvature $\|\nabla_{\mathbf{x}}(\hat{f}_{1_\varphi})\|\kappa$ controlled by a projection $\mathfrak{P} : \ell^2(\Lambda) \rightarrow \ell^2(\Lambda)$ through $\Gamma$ on the data constraints provided by the observation model, represented by $\mathfrak{P} = H^{\mathrm{T}}(H\hat{\mathbf{f}}_1 - \mathbf{f}_2)$. Hence, the speed $\nu_d$ of the LSM provided in (10) provides a descent solution scheme to the minimization problem of $\mathcal{J}_d$ as commonly used in gradient descent methods, whereas the speed $\nu_s$ plays a role that is akin to the minimization of $\mathcal{J}_s$ as given in Section II-C.

Although the total variation in (9) is convex [50], it is nondifferentiable at points $\{\mathbf{x} \in \mathcal{W} : \|\nabla_{\mathbf{x}} f\| = 0\}$ where the spatial gradient vanishes as in regions with constant grey value or for constant images [51]. Consequently, arriving at the unique minimizer of (9) becomes a numerically arduous problem. The exact solution in [31] is $\nu_s = \kappa / \|\nabla_{\mathbf{x}}(\hat{f}_{1_\varphi})\|$ which has proven to provide a stiff solution and it was suggested in the literature that it be preconditioned by multiplying by $\|\nabla_{\mathbf{x}}(\hat{f}_{1_\varphi})\|$. However, in the literature, the exact $\nu_d$ as given in (10) was multiplied as well by $\|\nabla_{\mathbf{x}}(\hat{f}_{1_\varphi})\|$, which is unnecessary and led to a solution scheme with all the constant images as its minimizers, the need for a stopping criterion to the iterations, and with the solution dependent on the initial guess $\hat{f}_1^{(0)}$. Hence, we formulated the solution scheme using the proposed speeds in (10) which has a unique nonconstant image minimizer (unless $f_2$ is a constant image), independent of the initial guess $\hat{f}_1^{(0)}$, and which does not need a special stopping criterion because the solution method converges to a unique solution.

It can be shown that the objective function (9) is convex, but not strictly convex. It has a unique minimizer as long as no nonzero constant vectors lie in the null space of $H$. This is reasonable since $H$ incorporates a low-pass filter with nonzero DC gain. Note that convergence of our algorithm to this unique minimizer was only justified empirically by running the solution scheme with the following cases.

- Different initial guesses, such as zero image, constant image, and a random image generated from a Gaussian distribution and cropped to the grayscale range ([0, 1]) of an image were used, and the method always converged to the same solution.
- In simulated experiments to the scenario of Fig. 2, a very high-resolution image was down-sampled twice by large factors (25 and 625) to generate an ideal HR image $f_1$ and the observation LR image $f_2$. The ideal $f_1$ was then used as initial guess and the method always converged to the same solution that is obtained by starting with any other initial guess. Although the solution obtained in this case is visually worse than the initial ideal HR guess, it supports uniqueness of the solution and independence of the initial guess.

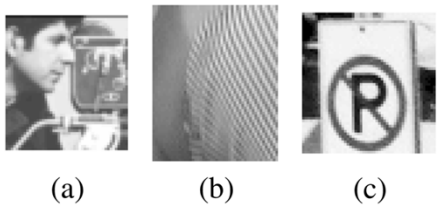


Fig. 7. Original LR images. (a) Portion of the cameraman image. (b) Portion of the Barbara image. (c) Parking sign image.

## V. Perceptual Uniformity Versus Linearity

The output light of cathode ray tubes (CRTs) is related to the input image by the power law [52]; images are raised to the power of a constant $(\gamma)$ by the CRT. Hence, in order to display images correctly on CRTs, they need to be compensated for this effect by preprocessing them. This compensation process is known as gamma correction. The gamma correction is normally performed automatically by physical cameras so that the digital image obtained is ready to be fed directly to the CRT. A commonly used gamma correction for CRTs is the ITU-R Rec. 709 given by

$$f^{(\gamma)} = \begin{cases} 4.5f, & f \leq 0.018 \\ 1.099f^{0.45} - 0.99, & 0.018 < f \leq 1. \end{cases}$$

An advantage associated with the gamma correction process is that it produces images that are considered to be approximately perceptually uniform. The gamma correction process is nonlinear but our observation model in Section III is applicable to linear-shift invariant (LSI) systems. This means that we need to perform our processing on the nongamma-corrected image while maintaining an approximately perceptually uniform space in accordance with the properties of the human visual system (HVS).


Fig. 8. Up-sampling of a portion of the cameraman image in Fig. 7(a) by a factor of 25 using (a) the proposed approach $\lambda = 0.025$, (b) the total-variation method in [25], and (c) cubic *B*-spline. (d) A portion of the cameraman image obtained directly by down-sampling from the original image by a factor of 25 using a Gaussian camera model prefilter.

In order to solve this problem, we developed a methodology that performed all the processing in the linear grayscale space while correcting for the perceptual uniformity using the gamma correction. This is done by obtaining a correction weight that depends on the grayscale value of the sample to be processed. Let us denote the gamma-corrected image by $f^{(\gamma)}$ and the distance between two grayscale values as $\Delta E$ and $\Delta E_\gamma$ in the grayscale and the gamma-corrected space, respectively. The correction weight that maps the measure $\Delta E$ to its corresponding $\Delta E_\gamma$, for small values of $\Delta E$, can be obtained simply by computing $\partial f^{(\gamma)}/(\partial f)$ and is given by

$$\frac{\partial f^{(\gamma)}}{\partial f} = \begin{cases} 4.5, & f \leq 0.018 \\ 0.49/f^{0.55}, & 0.018 < f \leq 1. \end{cases}$$

Hence, we can write the corrected distance $\Delta E_{\text{cor}}$ that approximates $\Delta E_\gamma$ as

$$\Delta E_{\text{cor}} = \frac{\partial f(\gamma)}{\partial f} \Delta E. \tag{12}$$

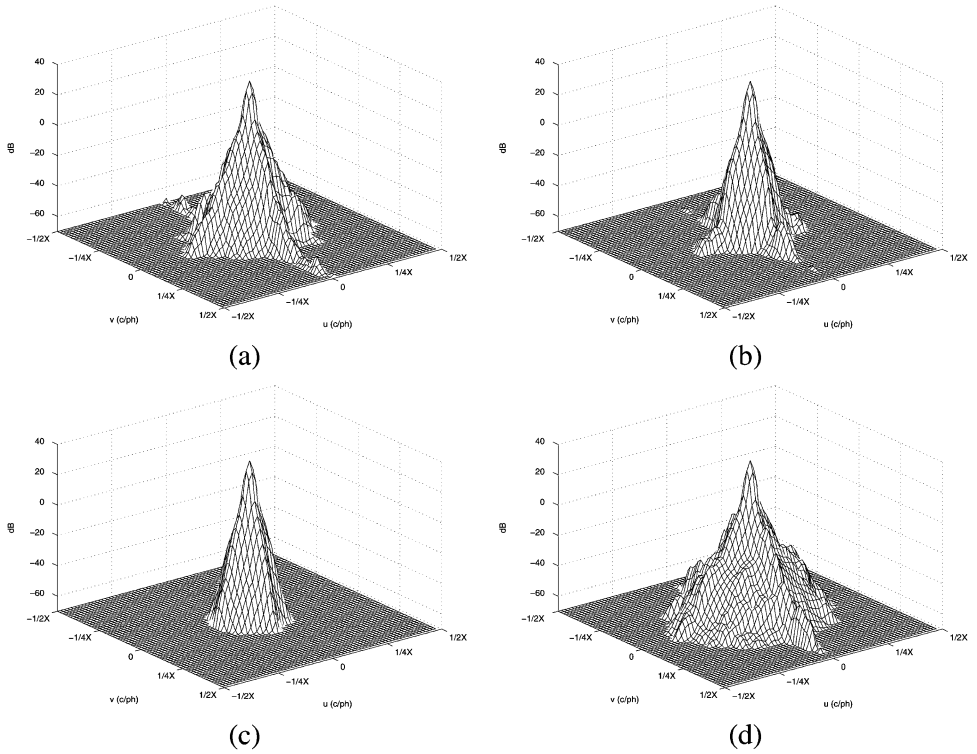


Fig. 9. Estimation of the PSD of the up-sampled cameraman image by a factor of 25 using (a) the proposed approach $\lambda = 0.025$ and (b) total variation in [25] (c) cubic B-spline, and (d) that of the ideal HR image.

We computed these weights for a reasonable step to quantize the grayscale range [0, 1] and then stored them in a look-up table (LUT). This LUT is then used by any image-processing algorithm to correct the updates of samples during the processing. We used these correction weights in image up-sampling and it resulted in subtle enhancements near the edges. It should be noted that the procedure described here can equally be applied on the $L^*$ channel used in the CIELAB color space, which is more perceptually uniform than the gamma-corrected grayscale. The reason that we used the gamma-corrected processing is just for convenience because generally digital images are provided in the gamma-corrected space.

## VI. Implementation Algorithms

The implementation of our grayscale regularized image up-sampling is described by the following algorithms. The main algorithm is also illustrated in block-diagram form in Fig. 6.

Algorithm 1: Image up-sampling $(f_2, \lambda, \Delta T, \epsilon)$

1) Undo the gamma-correction to $f_2$.
2) Initialize $f_1^{(0)}$ by any arbitrary image.
3) Set $n = -1$.
4) Do until termination criterion is satisfied:
   a) $n = n + 1$;
   b) estimate the preconditioned mean curvature $\|\nabla_{\mathbf{x}} f_1^{(n)}\|\kappa^{(n)}$ by Algorithm 2.
   c) Compute the error $e^{(n)} = H\mathbf{f}_1^{(n)} - \mathbf{f}_2$ as in Fig. 6.
   d) Compute the residue $r^{(n)} = H^{\mathrm{T}} e^{(n)}$ as shown in Fig. 6.
   e) $\zeta^{(n)} = (\partial f_1^{(\gamma)})/(\partial f_1)^{(n)}$.
   f) $f_1^{(n+1)} = f_1^{(n)} + \zeta^{(n)} \Delta T(\lambda \|\nabla_{\mathbf{x}} f_1^{(n)}\|\kappa^{(n)} - r^{(n)})$.
   g) Compute the termination criterion $\mathrm{MSE}(f_1^{(n+1)}, f_1^{(n)}) < \epsilon$.
5) Gamma-correct $f^{(n)}$ and Store it as $\hat{f}_1$.

The preconditioned mean curvature can be computed using central finite differences or analytically in terms of a specific prototype basis function $\varphi$. This function serves as the basis of an embedding space over $\Lambda$. This gives the freedom to use many different prototype functions $\varphi$ like sinc, spline, or any other that combines the cascade effect of the display device used and an approximated LSI response of the HVS.

Algorithm 2: Preconditioned mean curvature $(f)$.

1) Estimate the partial derivatives: $f_x, f_y, f_{xx}, f_{yy}, f_{xy}$ as in Appendix A. I or
   A. II
2) Estimate $\|\nabla_{\mathbf{x}} f\| = \sqrt{f_x^2 + f_y^2}$
3) If $\|\nabla_{\mathbf{x}} f\| = 0$ then set $\|\nabla_{\mathbf{x}} f\|\kappa = 0$
4) Else set $\|\nabla_{\mathbf{x}} f\|\kappa = (f_{xx} f_y^2 - 2 f_x f_y f_{xy} + f_{yy} f_x^2)/(f_x^2 + f_y^2)$
5) Return $\|\nabla_{\mathbf{x}} f\|\kappa$.

Since $\mathcal{J}_s$ given in (9), is nondifferentiable at $\|\nabla_{\mathbf{x}} f\| = 0$, then we set $\|\nabla_{\mathbf{x}} f\|\kappa = 0$ in Algorithm 2. This remedy is prescribed in [51], [40] where we resort to the subgradient of the objective function $(\mathcal{J}_d')$. This treatment is totally different from the common straightforward approximation $\|\nabla_{\mathbf{x}} f\| = \sqrt{f_x^2 + f_y^2 + \epsilon}$ for small value $\epsilon$; details can be found in [36].

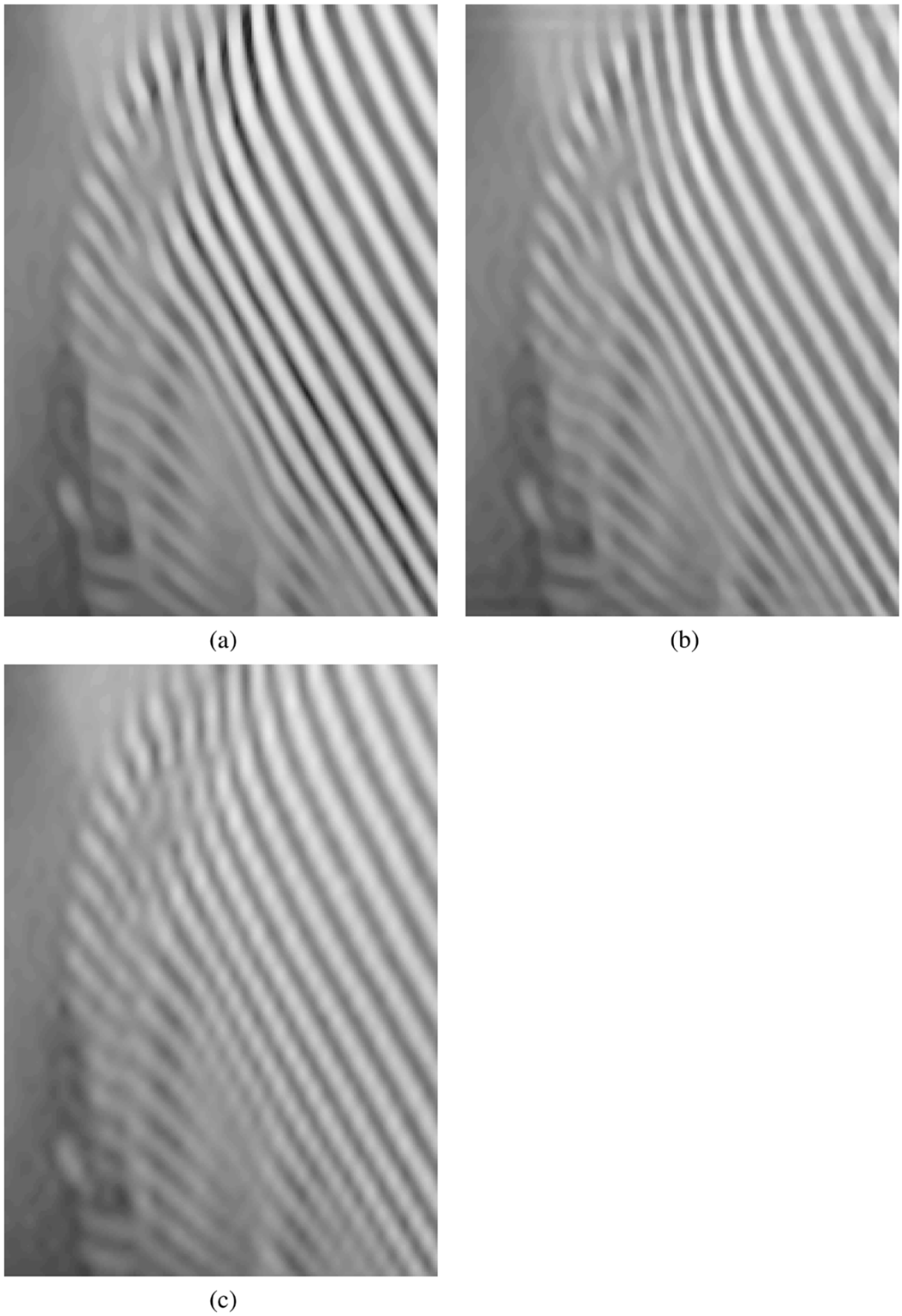


Fig. 10. Up-sampling the image in Fig. 7(b) by a factor of 25 using (a) the proposed approach $\lambda = 0.15$, (b) the total-variation method in [25], and (c) cubic B-spline.

## VII. Experiments and Results

In this section, we present some sample results for grayscale image up-sampling using the proposed approach in (9). The solution scheme is implemented using hybrid LSMs interacting simultaneously that are given by (10). The iterative numerical implementation of the LSM given by (11) is implemented using Algorithms 1 and 2. The choice of the regularization parameter was based on subjective quality by running the experiments for several values of $\lambda$, where the subjective quality of the results was assessed informally by our personal preference as human viewers in terms of edge sharpness, contour crispness, no ringing in smooth regions, and no ringing near edges. Different choices for the regularization parameter yield visually

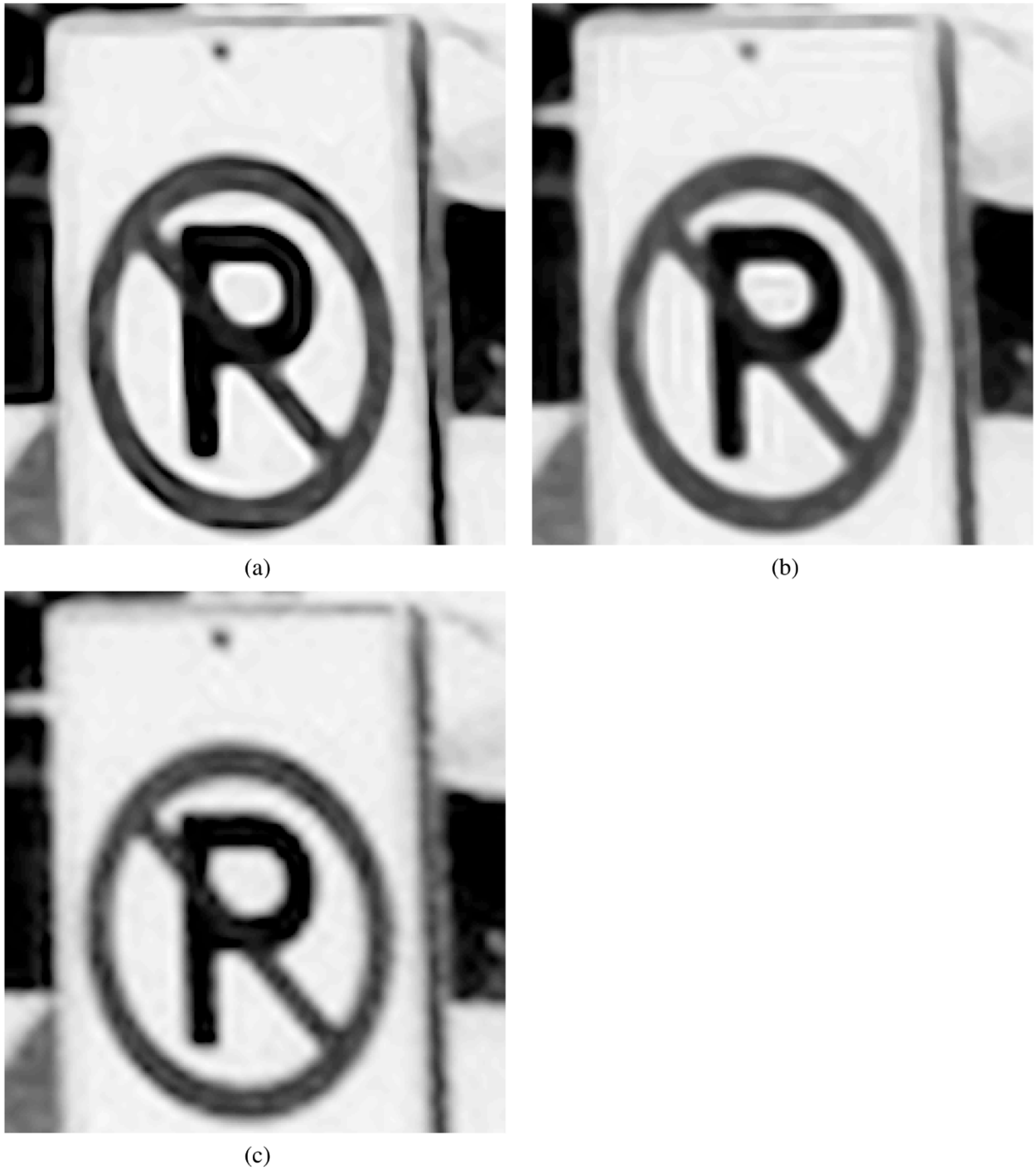


Fig. 11. Up-sampling the image in Fig. 7(c) by a factor of 25 using (a) the proposed approach $\lambda = 0.1$, (b) the total-variation method in [25], and (c) cubic B-spline.

different results. All these results for $\lambda$ in a certain range ([0.01, 0.2]) are better from a perceptual point of view than other techniques such as the total-variation method in [25] and cubic B-spline. The sampling structures $\Lambda \supset \Gamma$ used are both rectangular and $\Lambda$ is assumed to be five times denser than $\Gamma$ in each dimension. The scenario used to design the observation model for up-sampling is assumed to be Gaussian for both $h_1$ and $h_2$, denoted by Gauss–Gauss($\downarrow 25$). The iterative process was run until convergence was achieved, normally within a few hundred iterations. However, the convergence for sharp step edges and ramp edges is slower and may take up to a few thousand iterations in some cases.

It should be noted that we do not have any knowledge about the acquisition process for the LR images in most of these experiments. Since we first need to run a controlled simulated experiment to obtain peak signal-to-noise ratio (PSNR) figures, we simulated the scenario given in Fig. 2. We chose the Gauss–Gauss($\downarrow 25$) scenario, and we started with a very-high-resolution version of an original photograph of the MIT Research Laboratory of Electronics standard image

"cameraman" of size $6 \times 6$ in acquired by a 1200 dpi scanner to produce a $7200 \times 7200$ image. We filtered the image produced with two Gaussian filters simulating $h_1$ and $h_2$ and then subsampled by two different factors, 625 and 25, simulating sampling on $\Lambda$ and $\Gamma$, respectively. A crop from the resulting LR image $f_2$ is shown in Fig. 7(a) while the same crop of the ideal HR image $f_1$ is shown in Fig. 8(d). We up-sampled the image given in Fig. 7(a) using the proposed approach for $\lambda = 0.025$, where convergence was achieved after 1000 iterations and the result is shown in Fig. 8(a). The result was also obtained using an enhanced implementation of the total-variation method in [25] using speeds for the evolution of the LSM analogous to our enhanced speeds as shown in Fig. 8(b) and cubic *B*-spline as shown in Fig. 8(c).

The results using the proposed method show enhancement over both other methods in many aspects. The measured mean-squared error difference between the ideal HR image and the up-sampled images is expressed in PSNR. For the proposed approach, we obtained 22.86 dB; for the method in [25], we obtained 22.39 dB; and for cubic *B*-spline, we obtained 22.02 dB. Although the resulting up-sampled images have significant visual differences, their PSNR values with respect to the ideal image differ by only less than 1 dB. This indicates that PSNR figures are not a suitable metric for image up-sampling, especially for large up-sampling factors. As an alternative, we recommend visualizing an estimation of the PSD of the up-sampled images and see how much of the spectrum is extrapolated in $\mathcal{P}_{\Lambda^*} \setminus \mathcal{P}_{\Gamma^*}$ in a consistent manner, as shown in Fig. 9. PSD estimates of the up-sampled cameraman image using the proposed approach, the method in [25], and cubic *B*-spline are shown in Fig. 9(a)–(c), along with that for the ideal HR image, shown in Fig. 9(d). It is clear that more useful spatial frequencies are extrapolated (synthesized) using the proposed approach than the other two methods.

Since the problem is direct up-sampling of given LR images without incorporating other simulation effects like down-sampling, we directly up-sampled LR images. We compare them visually and inspect their PSD instead of PSNR figures, which are not available now because an ideal HR image does not exist.

The first example is up-sampling a portion of Barbara image shown in Fig. 7(b) using the proposed approach [Fig. 10(a)], the total-variation method in [25] [Fig. 10(b)], and cubic B-spline Fig. 10(c). The parameters used in the result in Fig. 10(a) are $\lambda = 0.15$ and Gauss–Gauss$(\downarrow 25)$ scenario. It is clear from the figures that results obtained with the proposed approach are better than the results by the total-variation method in [25]. The stripes are sharper without any ringing compared to the result in Fig. 10(b). The hand on the left side of the image is smooth in Fig. 10(a) while it suffers from some ringing in Fig. 10(b). The result of using the cubic B-spline presented in Fig. 10(c) shows significant ringing along the stripes, and it is not as sharp as the one in Fig. 10(a). The second example is up-sampling a parking-sign image, which is a portion of a $3 \times 5$-in black-and-white glossy photo scanned at 300 dpi [Fig. 7(c)], using our proposed approach, the total-variation method in [25], and cubic B-spline. The results are shown in Fig. 11(a)–(c). It is clear that our method results in an up-sampled image with the fewest spurious patterns. In the cubic B-spline result, the boundaries of the text suffer from artifacts that makes visualization difficult. Although the result of the total-variation method in [25] is better than that of spline, it suffers from ringing in the smooth white background closer to vertical and horizontal edges such as those of the letter "P" and the outer border of the sign. We tried different values for $\lambda$ and based on our experimental experience we recommend using $\lambda \in [0.01, 0.2]$ as a tuning parameter left to the user preference. The effect of the values of $\lambda$ on total-variation regularization is analyzed in [37]. It should be noted that the effect of the perceptual uniformity development of Section V provided a subtle enhancement to the results.

The main drawback of the proposed approach, due to its iterative nature, is the computation time. Specifically, the main burden in the computation is the estimation of the mean curvature $\kappa$. Its computation requires the estimation of five partial derivatives which are implemented by convolutions with different kernel sizes, computation of the squares of both $f_x, f_y$, and performing an additional four multiplications, three additions, and one division. This drawback can be mitigated by hardware implementation since the computation is localized in a small neighborhood around the target pixel. Another way to enhance the speed is by mathematical inspection of the problem and determining a better optimization technique. Fortunately, there is a recent work in [53], [54] to solve these kinds of optimization problems numerically in the dual space. They implemented this dual space numerical optimization for quadratic-type objective functions for signal restoration [53]. This seems to be a promising mathematical result to reduce the current computational load. Implementation of this new optimization method is still needed for the total-variation norm like the one we are using in this paper.

## VIII. Conclusion

This paper presents a new formulation of the regularized image up-sampling problem that incorporates models of the image acquisition processes at the different sampling densities and of the display process. A new analytic perspective is introduced, based on an analysis that justifies the use of total-variation regularizer that specifies the requirements of edge-directed filtering. This approach leads to a new data fidelity term that has been coupled with a total-variation regularizer to yield our objective function. This objective function is minimized using a LSM, based on the level set method, with two types of motion that interact simultaneously. A new choice of the motions of the level-sets led to a stable solution scheme that has a unique solution. Whereas other choices of the speeds used in the LSM formulation of this problem may result in being trapped in suboptimal stationary points, the motions used in this paper provided a stable solution which could be started from arbitrary initial conditions including constant images. An aspect of the human vision system, perceptual uniformity, is treated in accordance with the linear nature of the data fidelity term. The method was implemented in software and was verified to provide good results, yielding crisp edges without introducing ringing or other artifacts.

## APPENDIX I
## ESTIMATION OF PARTIAL DERIVATIVES USING FINITE DIFFERENCES

The numerical implementations of the partial derivatives in the mean curvature term $\kappa$ is the most critical and tricky part. "Generally the numerical implementation of PDEs should take into account the domain of dependence of the underlying data" [50]. In the case of the parabolic term $\kappa$, the domain of dependence is all the surrounding spatial data with no bias toward a specific direction [35]. Hence, the most suitable discretization advised by the authors of [50], [39] for the curvature term is the second-order central differences. We have five partial derivatives to implement. These partial derivatives can be efficiently implemented by a simple convolution process. Thus, the second-order approximation of the partial derivatives becomes $\hat{\tilde{f}}_{1_{(.)}}(\mathbf{d}) = \hat{f}_1[\mathbf{d}] * h_{(.)}[\mathbf{d}], \forall \mathbf{d} \in \Lambda$. The impulse responses of the filters $h_{(.)}[\mathbf{d}]$ for the implementation of each of the partial derivatives are given by

$$\begin{aligned} h_x &= [0.5 \quad \mathbf{0} \quad -0.5], \quad h_y = h_x^{\mathrm{T}} \\ h_{xx} &= [1 \quad \mathbf{-2} \quad 1], \quad h_{yy} = h_{xx}^{\mathrm{T}} \\ h_{xy} &= h_y \cdot h_x. \end{aligned} \tag{13}$$

The bold number indicates the central position $\mathbf{x} = \mathbf{0}$. It should be noted that we are using a top-to-bottom orientation, i.e., the positive vertical direction points downwards.

## APPENDIX II
## ESTIMATION OF THE PARTIAL DERIVATIVES ANALYTICALLY

The spatial partial derivatives can be analytically derived in the spatial domain using a prototype embedding function $\varphi$ as in (9) where the partial derivatives can be analytically evaluated by

$$(\hat{f}_{\varphi})_{(.)}(\mathbf{x}) = \sum_{\mathbf{d} \in \Lambda} \hat{f}[\mathbf{d}] \varphi_{(.)}(\mathbf{x} - \mathbf{d}), \quad \forall \mathbf{x} \in \mathcal{W}. \tag{14}$$

It is clear that if we have an analytic continuous model $\varphi$ such as the display device used cascaded with the properties of the HVS, spline, or simply a sinc function, then we can compute the partial derivatives for all $\mathbf{x} \in \mathcal{W}$ and not only on $\Lambda$. If we inspect (14), we find that the value of the partial derivative at any position $\mathbf{x} \in \mathcal{W}$ is theoretically dependent on all the samples of $\hat{f}[\mathbf{d}]$. However, when $\varphi(\mathbf{x} - \mathbf{d}), \forall \mathbf{d} \in \Lambda$ decays quickly providing a compact support function, which is the case for spline and practical display devices, we only need to perform the summation in (14) for a small number of samples depending on the order of the accuracy required. This leads to the fact that we can numerically approximate (14) at points of $\Lambda$ using a simple convolution process as follows:

$$\begin{aligned} (\hat{f}_{\varphi})_{(.)}(\mathbf{d}) &= \hat{f}_1[\mathbf{d}] * h_{(.)}[\mathbf{d}], \\ h_{(.)}[\mathbf{d}] &= \varphi_{(.)}(\mathbf{d}), \quad \mathbf{d} \in \Lambda. \end{aligned} \tag{15}$$

## REFERENCES


[1] E. DuBois, "Video sampling and interpolation," in *Handbook of Image and Video Processing*, A. Bovik, Ed. San Diego, CA: Academic, 2000, ch. 7.2, pp. 645–654. E. Dubois, "Video sampling and interpolation".

[2] E. Dubois, "The sampling and reconstruction of time-varying imagery with application in video systems," *Proc. IEEE*, vol. 73, no. 4, pp. 502–522, Apr. 1985.

[3] R. Keys, "Cubic convolution interpolation for digital image processing," *IEEE Trans. Acoust. Speech, Signal, Process.*, vol. ASSP-29, no. 6, pp. 1153–1160, Dec. 1981.

[4] A. Muñoz, T. Blu, and M. Unser, "Least-squares image resizing using finite differences," *IEEE Trans. Image Process.*, vol. 10, no. 9, pp. 1365–1378, Sep. 2001.

[5] M. Unser, "Splines: A perfect fit for signal and image processing," *IEEE Signal Process. Mag.*, vol. 16, no. 6, pp. 22–38, Nov. 1999.

[6] A. Gotchev, K. Egiazarian, J. Vesma, and T. Saramäki, "Edge-preserving image resizing using modified B-splines," in *Proc. IEEE Int. Conf. Acoustics, Speech, Signal Processing*, vol. 3, 2001, pp. 1865–1868.

[7] T. Blu, P. Thévenaz, and M. Unser, "Linear interpolation revitalized," *IEEE Trans. Image Process.*, vol. 13, no. 5, pp. 710–719, May 2004.

[8] Q. Wang, R. Ward, and H. Shi, "Isophote estimation by cubic-spline interpolation," in *Proc. IEEE Int. Conf. Image Processing*, vol. 3, 2002, pp. 401–404.

[9] J. P. Allebach, "Image scanning, sampling, and interpolation," in *Handbook of Image and Video Processing*, A. Bovik, Ed. San Diego, CA: Academic, 2000, ch. 7.1, pp. 629–643.

[10] A. Biancardi, L. Cinque, and L. Lombardi, "Improvements to image magnification," *Pattern Recognit.*, vol. 35, pp. 677–687, Mar. 2002.

[11] S. Carrato, G. Ramponi, and S. Marsi, "A simple edge-sensitive image interpolation filter," in *Proc. IEEE Int. Conf. Image Processing*, vol. 3, 1996, pp. 711–714.

[12] Q. Wang and R. Ward, "A new edge-directed image expansion scheme," in *Proc. IEEE Int. Conf. Image Processing*, vol. 3, 2001, pp. 899–902.

[13] W. K. Carrey, D. B. Chuang, and S. S. Hemami, "Regularity-preserving image interpolation," *IEEE Trans. Image Process.*, vol. 8, no. 9, pp. 1293–1297, Sep. 1999.

[14] T. Chen, H. R. Wu, and B. Qiu, "Image interpolation using across-scale pixel correlation," in *Proc. IEEE Int. Conf. Acoustics Speech Signal Processing*, vol. 3, 2001, pp. 1857–1860.

[15] X. Li and T. Orchard, "New edge-directed interpolation," *IEEE Trans. Image Process.*, vol. 10, no. 10, pp. 1521–1527, Oct. 2001.

[16] Y. Takahashi and A. Taguchi, "An enlargement method of digital images with the prediction of high-frequency components," in *Proc. IEEE Int. Conf. Acoustics, Speech, Signal Processing*, vol. 4, 2002, pp. 3700–3703.

[17] A. Darwish, M. Bedair, and S. Shaheen, "Adaptive resampling algorithm for image zooming," *Proc. Inst. Elect. Eng. Vis., Image, Signal Process.*, vol. 144, pp. 207–212, Aug. 1997.

[18] H. A. Aly and E. Dubois, "Specification of the observation model for regularized image up-sampling," *IEEE Trans. Image Process.*, vol. 14, no. 5, pp. 567–576, May 2005.

[19] G. Golub and C. V. Loan, *Matrix Computations*, 3rd ed. Baltimore, MD: Johns Hopkins Univ. Press, 1996.

[20] J. Hadamard, *Lectures on Cauchy's Problem in Linear Partial Differential Equations*. New York: Dover, 1952.

[21] R. R. Schulz and R. L. Stevenson, "A Bayesian approach to image expansion for improved definition," *IEEE Trans. Image Process.*, vol. 3, no. 5, pp. 233–242, May 1994.

[22] S. Geman and D. Geman, "Stochastic relaxation, Gibbs distributions', and the Bayesian restoration of images," *IEEE Trans. Pattern Anal. Mach. Intell.*, vol. PAMI-6, no. 7, pp. 721–741, Jul. 1984.

[23] D. Rajan and S. Chaudhuri, "Generation of super-resolution images from blurred observations using Markov random fields," in *Proc. IEEE Int. Conf. Acoustics, Speech, Signal Processing*, vol. 3, 2001, pp. 1837–1840.

[24] C. Bouman and K. Sauer, "A generalized Gaussian image model for edge-preserving MAP estimation," *IEEE Trans. Image Process.*, vol. 2, no. 7, pp. 296–310, Jul. 1993.

[25] F. Malgouyres and F. Guichard, "Edge direction preserving image zooming: A mathematical and numerical analysis," *SIAM J. Numer. Anal.*, vol. 39, pp. 1–37, 2001.

[26] B. Morse and D. Schwartzwald, "Image magnification using level-set reconstruction," in *Proc. IEEE Conf. Computer Vision Pattern Recognition*, vol. 1, 2001, pp. 333–340.

[27] W. C. Karl, "Regularization in image restoration and reconstruction," in *Handbook of Image and Video Processing*, A. Bovik, Ed. San Diego, CA: Academic, 2000, ch. 3.6, pp. 141–160.

[28] P. D. Welch, "The use of fast Fourier transform for the estimation of power spectra: A method based on time averaging over short, modified periodograms," *IEEE Trans. Audio Electroacoust.*, vol. AU-15, pp. 70–73, Jun. 1967.

[29] E. Dubois, "Spectral analysis of image sequences," Institut national de la recherche scientifique (INRS), Montreal, QC, Canada, Tech. Rep. 83-03, Feb. 1983.
[30] P. Perona and J. Malik, "Scale-space and edge detection using anisotropic diffusion," *IEEE Trans. Pattern Anal. Mach. Intell.*, vol. 12, no. 7, pp. 629–639, Jul. 1990.
[31] L. Rudin, S. Osher, and E. Fatemi, "Nonlinear total variation based noise removal algorithms," *Phys. D*, vol. 60, pp. 259–268, 1992.
[32] L. Alvarez, P. Lions, and J. Morel, "Image selective smoothing and edge detection by nonlinear diffusion," *SIAM J. Numer. Anal.*, vol. 29, pp. 845–866, Jun. 1992.
[33] Y. You, W. Xu, A. Tannenbaum, and M. Kaveh, "Behavioral analysis of anisotropic diffusion in image processing," *IEEE Trans. Image Process.*, vol. 5, no. 11, pp. 1539–1552, Nov. 1996.
[34] M. Giaquinta and S. Hildebrandt, *Calculus of Variations*. New York: Springer-Verlag, 1996.
[35] W. F. Ames, *Numerical Methods for Partial Differential Equations*. London, U.K.: Nelson, 1969.
[36] H. A. Aly, "Regularized image up-sampling," Ph.D. dissertation, School Inf. Technol. Eng. (SITE), Univ. Ottawa, Ottawa, ON, Canada, Mar. 2004.
[37] D. Strong and T. Chan, "Edge-preserving and scale-dependent properties of total variation regularization," *Inv. Probl.*, vol. 19, pp. 165–187, 2003.
[38] S. Osher and J. Sethian, "Fronts propagating with curvature dependent speed: Algorithms based on the Hamilton-Jacobi formulation," *Comput. Phys. J.*, vol. 79, pp. 12–49, 1988.
[39] J. Sethian, *Level Set Methods and Fast Marching Methods*, 2nd ed. Cambridge, U.K.: Cambridge Univ. Press, 1999.
[40] A. Marquina and S. Osher, "Explicit algorithms for a new time dependent model based on level set motion for nonlinear deblurring and noise removal," *SIAM J. Sci. Comput.*, vol. 22, pp. 387–405, 2000.
[41] B. Tom and A. Katsaggelos, "Resolution enhancement of monochrome and color video using motion compensation," *IEEE Trans. Image Process.*, vol. 10, no. 2, pp. 278–287, Feb. 2001.
[42] S. Baker and T. Kanade, "Limits on super-resolution and how to break them," *IEEE Trans. Pattern Anal. Mach. Intell.*, vol. 24, no. 9, pp. 1167–1183, Sep. 2002.
[43] B. Morse and D. Schwartzwald, "Isophote-based interpolation," in *Proc. IEEE Int. Conf. Image Processing*, vol. 3, 1998, pp. 227–231.
[44] ——, "Image magnification using level-set reconstruction," in *Proc. IEEE Conf. Computer Vision Pattern Recognition*, vol. 1, 2001, pp. 333–340.
[45] H. Jiang and C. Moloney, "A new direction adaptive scheme for image interpolation," in *Proc. IEEE Int. Conf. Image Processing*, vol. 3, 2002, pp. 369–372.
[46] G. Gilboa, Y. Zeevi, and N. Sochen, "Anisotropic selective inverse diffusion for signal enhancement in the presence of noise," in *Proc. IEEE Int. Conf. Acoustics, Speech, Signal Processing*, vol. 1, Istanbul, Turkey, Jun. 2000, pp. 221–224.
[47] G. Gilboa, N. Sochen, and Y. Y. Zeevi, "Forward-and-backward diffusion processes for adaptive image enhancement and denoising," *IEEE Trans. Image Process.*, vol. 5, no. 7, pp. 689–703, Jul. 2002.
[48] S. Borman and R. L. Stevenson, "Super-resolution for image sequences—A review," in *Proc. IEEE Int. Symp. Circuits Systems*, 1998, pp. 374–378.
[49] H. Aly and E. Dubois, "Regularized image up-sampling using a new observation model and the level set method," in *Proc. IEEE Int. Conf. Image Processing*, vol. 3, 2003, pp. 665–668.
[50] S. Osher and R. Fedkiw, *Level Set Methods and Dynamic Implicit Surfaces*. New York: Springer-Verlag, 2003.
[51] P. L. Combettes and J. Luo, "An adaptive level set method for nondifferentiable constrained image recovery," *IEEE Trans. Image Process.*, vol. 11, no. 11, pp. 1295–1304, Nov. 2002.
[52] C. Poynton, *Digital Video and HDTV: Algorithms and Interfaces*. Amsterdam, The Netherlands: Morgan Kaufmann, 2003.
[53] P. L. Combettes, "A block-iterative surrogate constraint splitting method for quadratic signal recovery," *IEEE Trans. Signal Process.*, vol. 51, no. 7, pp. 1771–1782, Jul. 2003.
[54] H. H. Bauschke and P. L. Combettes, "Construction of best Bergman approximations in reflexive Banach spaces," in *Proc. Amer. Math. Soc.*, vol. 131, 2003, pp. 3757–3766.

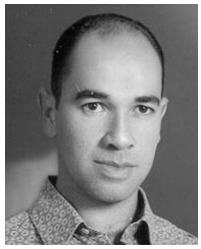

**Hussein A. Aly** (M'00) received the B.Sc. degree (excellent with honors) in computer engineering and the M.Sc. degree in electrical engineering from the Military Technical College, Cairo, Egypt, and the Ph.D. degree in electrical engineering from the University of Ottawa, Ottawa, ON, Canada, in 1993, 1997, and 2004, respectively.

He is currently with the Ministry of Defence, Cairo, Egypt. While at the University of Ottawa, he participated in a project on image magnification funded by the Royal Canadian Mounted Police (RCMP). His research interests are in image sampling theory and sampling structure conversion. His current research is focused on high-quality image magnification, interpolation of color filter array data (demosiacking), and the application of total variation for image processing.

Dr. Aly is a member of the Egypt Engineers Syndicate.

**Eric Dubois** (F'96) received the B.Eng. (honors, with great distinction) and M.Eng. degrees in electrical engineering from McGill University, Montreal, QC, Canada, and the Ph.D. degree in electrical engineering from the University of Toronto, Toronto, ON, Canada, in 1972, 1974, and 1978, respectively.

He joined the Institut National de la Recherche Scientifique, University of Quebec, Montreal, in 1977, where he held the position of Professor in the INRS-Télécommunications Centre, Montreal. Since July 1998, he has been a Professor with the School of Information Technology and Engineering (SITE), University of Ottawa, Ottawa, ON. He recently completed terms as Vice Dean and Secretary of the Faculty of Engineering. His research has centered on the compression and processing of still and moving images and in multidimensional digital signal processing theory. His current research is focused on archival document processing and compression, stereoscopic and multiview imaging, image sampling theory, and image-based virtual environments. The research is being carried out in collaboration with such organizations as the Communications Research Centre, the National Capital Institute of Telecommunications, the Royal Canadian Mounted Police (RCMP), and the Learning Objects Repositories Network (LORNET). He is a member of the editorial board of the EURASIP journal *Signal Processing: Image Communication*.

Dr. Dubois is corecipient of the 1988 Journal Award from the Society of Motion Picture and Television Engineers. He is a Fellow of the Engineering Institute of Canada, a Member of the Order of Engineers of Quebec, and was an Associate Editor of the IEEE TRANSACTIONS ON IMAGE PROCESSING (from 1994 to 1998). He was Technical Program Co-Chair for the IEEE 2000 International Conference on Image Processing (ICIP) and a member of the organizing committee for the IEEE 2004 ICASSP.